SymC Coupled-Oscillator Model of Neutrino Flavor Dynamics

Nate Christensen
SymC Universe Project — Missouri, USA
SymCUniverse@gmail.com

(Dated: November 2025)

Abstract

A unified dynamical model for neutrino oscillations is formulated within the Symmetrical Convergence (SymC) framework. Neutrinos are modeled as three damped oscillators (mass eigenmodes) coupled to a shared environmental channel, where misalignment between the flavor basis (where damping acts) and mass basis (where frequencies are diagonal) forces persistent oscillation. The formalism reproduces standard PMNS probabilities while adding a physically grounded interpretation of matter-dependent damping and exceptional points (EPs). **Vacuum propagation is strictly unitary**; all non-Hermitian effects are confined to matter segments where $\Gamma_f(x) \neq 0$. Predictions are falsifiable by JUNO, DUNE, and Hyper-Kamiokande.

Notation and units

Adopt beat-frequency notation

$$\varpi_k \equiv \frac{m_k^2}{2E}, \qquad \Omega_m^2 \equiv \mathrm{diag}(\varpi_1^2, \varpi_2^2, \varpi_3^2), \qquad \Gamma_f(x) = \mathrm{diag}(\gamma_e(x), \gamma_\mu(x), \gamma_\tau(x)),$$

and $\Gamma_m(x) = U^\dagger \Gamma_f(x) U$ in the mass basis. The SymC ratio for a mode is $\chi_k \equiv (\Gamma_m)_{kk}/(2\varpi_k)$. Energies are in GeV; 1 GeV $= 1.51927 \times 10^{24}\,\mathrm{s}^{-1} = 5.06773 \times 10^{15}\,\mathrm{km}^{-1}$. Natural units are used ($c = \hbar = 1$).

I. Core Equation

In natural units,

$$\ddot{\nu}_f + \Gamma_f \dot{\nu}_f + (\Omega_f^2 + 2EV_f)\nu_f = 0,$$

with $\nu_f = (\nu_e, \nu_\mu, \nu_\tau)^T$ and

$$\Omega_f^2 = U\,\Omega_m^2\,U^\dagger, \quad \Omega_m^2 = \mathrm{diag}(\varpi_1^2, \varpi_2^2, \varpi_3^2), \quad \varpi_k = \frac{m_k^2}{2E}, \quad \Gamma_f = \mathrm{diag}(\gamma_e, \gamma_\mu, \gamma_\tau),\ V_f = \mathrm{diag}(V_e, 0, 0).$$

In vacuum segments, set $\Gamma_f = 0$ exactly. Transforming to the mass basis,

$$\ddot{\nu}_m + \Gamma_m \dot{\nu}_m + \Omega_m^2 \nu_m = 0, \qquad \Gamma_m = U^\dagger \Gamma_f U.$$

II. Vacuum evolution (strictly unitary)

With $\Gamma_f \equiv 0$ in vacuum, flavor evolution reduces to the standard PMNS result. Defining $\Delta\varpi_{jk} = \Delta m_{jk}^2/(2E)$, the flavor transition probability is

$$P_{\alpha\to\beta}(L,E) = \delta_{\alpha\beta} - 4\sum_{j>k} \mathrm{Re}\big(U_{\alpha j}U_{\beta j}^* U_{\alpha k}^* U_{\beta k}\big) \sin^2\!\bigg(\frac{\Delta\varpi_{jk}L}{2}\bigg) + 2\sum_{j>k} \mathrm{Im}\big(U_{\alpha j}U_{\beta j}^* U_{\alpha k}^* U_{\beta k}\big) \sin\big(\Delta\varpi_{jk}L\big). \tag{1}$$

No exponential envelope multiplies (1); any damping appears only inside matter segments where $\Gamma_f(x) \neq 0$.

III. Matter and dissipative coupling

In matter:

$$\Omega_f^2 \to \Omega_f^2 + 2EV_f, \qquad \Gamma_f = \mathrm{diag}(\gamma_e, \gamma_\mu, \gamma_\tau), \quad \Gamma_m = U^\dagger \Gamma_f U.$$

Matter-loss structure

$$\kappa_{ij} = (\Gamma_m)_{ij} = \sum_\alpha U_{\alpha i}^* \gamma_\alpha U_{\alpha j}, \qquad \chi_k \simeq \frac{(\Gamma_m)_{kk}}{2\varpi_k}.$$

MSW resonance as an exceptional point

Near MSW resonance a 2×2 reduction of the non-Hermitian quadratic generator may exhibit an EP: the reduced characteristic polynomial discriminant vanishes, causing eigenvalue/eigenvector coalescence. In the Hermitian limit this reduces to $\Delta m^2 \cos 2\theta_v = 2EV_e$. Flavor-dependent damping shifts the discriminant locus; details and a worked example appear in Appendix B.

IV. No-Global-Critical Theorem

For ordered $\varpi_1 < \varpi_2 < \varpi_3$ and any matter profile where $(\Gamma_m)_{kk} > 0$ (derived from flavor-dependent Γ_f via $\Gamma_m = U^\dagger \Gamma_f U$),

$$\chi_k = \frac{(\Gamma_m)_{kk}}{2\varpi_k}.$$

Since the ϖ_k increase with mass eigenstate index while the $(\Gamma_m)_{kk}$ depend on the mixing matrix structure, no choice of density and energy simultaneously yields $\chi_1 = \chi_2 = \chi_3 = 1$.

Corollary: Under realistic flavor-dependent damping, the stationary configuration is a persistent multi-frequency beat. Oscillation is the equilibrium form of stability, provided $\chi_k < 1$ for all k.

V. Illustrative calibration and quantitative checks

Two illustrative normal-ordering cases at $E = 1$ GeV use $\Delta m^2_{21} = 7.42 \times 10^{-5}$ eV^2, $|\Delta m^2_{31}| = 2.50 \times 10^{-3}$ eV^2 (NuFIT central values). Convert 1 eV$^2 = 10^{-18}$ GeV^2.

Case A: $m_1 = 0.01$ eV; Case B: $m_1 \simeq 0$; $E = 1$ GeV. $\varpi_k = m_k^2/(2E)$ in GeV. Example matter dephasing $\Gamma_{\text{eff}} = 1 \times 10^{-23}$ GeV gives $\chi_k = \Gamma_{\text{eff}}/(2\varpi_k)$.

	m_k^2 [eV^2]	ϖ_k [GeV]	χ_k (Case A)	χ_k (Case B)
$k = 1$	1.00×10^{-4} (A) / 0 (B)	5.0×10^{-23} (A) / 0 (B)	~ 0.10	n/a
$k = 2$	1.742×10^{-4} (A) / 7.42×10^{-5} (B)	8.71×10^{-23} (A) / 3.71×10^{-23} (B)	~ 0.057	~ 0.135
$k = 3$	2.60×10^{-3} (A) / 2.50×10^{-3} (B)	1.30×10^{-21} (A) / 1.25×10^{-21} (B)	~ 0.0038	~ 0.0040

Nonunitarity estimate. For a representative Earth density segment with $\Gamma_{\text{eff}} = 10^{-23}$ GeV and standard PMNS parameters, the induced biorthogonal deviation satisfies a conservative bound

$$\| \Delta \|_\infty \equiv \| U_{\text{eff}} U_{\text{eff}}^\dagger - I \|_\infty \lesssim 10^{-4}.$$

This is negligible for current long-baseline sensitivities but nonzero in principle.

VI. Probability interpretation: dephasing vs absorption

Here, $\Gamma_f(x)$ models *phase-randomizing dephasing* in the flavor basis (trace-preserving). Interference terms attenuate while total probability remains unity across a matter segment. True *absorption* would correspond to non-trace-preserving channels and appears as a deficit that cannot be restored by basis rotation. Experimental separation: dephasing suppresses oscillation contrast without net loss; absorption produces an energy-dependent rate-like disappearance.

VII. Experimental roadmap and falsification criteria

The SymC framework makes six quantitative predictions falsifiable by current and near-future experiments. Each prediction specifies an observable, the expected signature, the responsible experiment, and the timeline for validation or refutation.

A. JUNO reactor neutrino spectrum (2025–2027)

Observable: Reactor $\bar{\nu}_e$ disappearance spectrum at $L \simeq 53$ km baseline.

Standard prediction: Pure oscillatory structure determined by Δm^2_{21} and Δm^2_{31} with no envelope.

SymC prediction: *Matter-segment envelope* with effective $\Gamma_{\text{eff}}(x)$ set by Earth crust density ($\rho \sim 2.6$ g/cm^3). For illustrative Case B ($m_1 \simeq 0$, $\Gamma_{\text{eff}} = 10^{-23}$ GeV), the envelope factor over 53 km baseline is

$$\exp(-\Gamma_{\text{eff}} L) \simeq \exp\bigl(-5.3 \times 10^{-7}\bigr) \simeq 1 - 5.3 \times 10^{-7},$$

yielding a fractional suppression of oscillation amplitude at $\mathcal{O}(10^{-7})$ level. This is *below* JUNO's energy resolution sensitivity but establishes an upper bound: $\Gamma_{\text{eff}} < 10^{-22}$ GeV implies $\chi_2 < 1.35$ (critically damped limit).

Falsification criterion: If JUNO observes spectral distortions consistent with $\Gamma_{\text{eff}} > 10^{-22}$ GeV that *cannot* be explained by standard matter effects, SymC envelope is confirmed. Conversely, if JUNO finds perfect agreement with unmodified oscillations to $< 10^{-7}$ precision, this places stringent bounds on $\gamma_e(x)$ in Earth crust.

Timeline: JUNO first physics results expected 2025–2026; full statistics by 2027.

B. DUNE long-baseline appearance and disappearance (2028–2031)

Observable: $\nu_\mu \to \nu_e$ appearance and $\nu_\mu \to \nu_\mu$ disappearance over $L = 1300$ km baseline with Near Detector (ND) at 574 m and Far Detector (FD) at Sanford Lab.

Standard prediction: Three-flavor oscillations with MSW matter enhancement in Earth's mantle; no additional coherence loss.

SymC prediction:

- **Near Detector (ND):** Vacuum segment; $\Gamma_f = 0$ exactly. Unmodified PMNS probabilities.
- **Far Detector (FD):** Mixed vacuum/matter path. Effective matter segments totaling $\sim$ 800 km at average mantle density $\rho \sim 4.5$ g/cm^3. For $\Gamma_{\text{eff}} = 3 \times 10^{-23}$ GeV (conservative Case B-like), envelope factor:

$$\exp(-\Gamma_{\text{eff}} \times 800 \text{ km}) = \exp\big(-1.2 \times 10^{-6}\big) \simeq 1 - 1.2 \times 10^{-6}.$$

- **ND/FD ratio:** The ratio of observed event rates corrects for flux normalization but reveals coherence loss. SymC predicts a *baseline-dependent suppression* scaling as $\exp(-\Gamma_{\text{eff}} L_{\text{matter}})$, distinct from energy-dependent absorption.

Critical test: DUNE's multi-GeV beam samples $E \sim$ 1–5 GeV. Since $\chi_k \propto E/m_k^2$, higher energies push χ_3 toward criticality. If $E = 3$ GeV and $\Gamma_{\text{eff}} = 10^{-22}$ GeV, then $\chi_3 \simeq 0.012$ (underdamped) while $\chi_2 \simeq 0.4$ (still oscillatory). The *mass-dependent* damping hierarchy $\chi_1 > \chi_2 > \chi_3$ produces a *spectral tilt* in the oscillation envelope that is unique to SymC.

Falsification criterion:

1. If DUNE observes ND/FD event-rate ratios consistent with pure oscillations (no envelope) to $< 10^{-6}$ precision across all energies, SymC envelope is ruled out at these densities.
2. If DUNE finds a baseline-dependent suppression that scales as predicted by $\exp(-\Gamma_{\text{eff}} L_{\text{matter}})$ and exhibits the χ_k hierarchy, this is direct evidence for SymC dephasing.

Timeline: DUNE beam start 2028; first oscillation results 2029–2030; precision measurements by 2031.

C. Hyper-Kamiokande atmospheric neutrinos (2027–2035)

Observable: Atmospheric ν_μ and $\bar{\nu}_\mu$ disappearance over baselines $L \sim$ 500–12,000 km (zenith-angle dependent).

Standard prediction: Energy- and zenith-angle-dependent oscillations with MSW resonance enhancement for upward-going neutrinos traversing Earth's core.

SymC prediction:

- **Downward-going** ($\cos\theta_z > 0$): Short atmospheric path; $\Gamma_f \simeq 0$. Standard PMNS.
- **Horizontal** ($\cos\theta_z \simeq 0$): Mixed vacuum/crust propagation; modest envelope.
- **Upward-going** ($\cos\theta_z < 0$): Long matter path through mantle and core ($\rho_{\text{core}} \sim$ 13 g/cm^3). Core densities amplify $\Gamma_{\text{eff}}(x)$ if damping scales with electron density (as expected for $\gamma_e \propto n_e$).

For core-crossing neutrinos with $L_{\text{core}} \sim 2500$ km and $\Gamma_{\text{core}} \sim 5 \times 10^{-23}$ GeV (extrapolated from mantle), envelope factor:

$$\exp(-\Gamma_{\text{core}} \times 2500\text{ km}) = \exp\bigl(-6.3 \times 10^{-6}\bigr) \simeq 1 - 6.3 \times 10^{-6}.$$

Critical signature: SymC predicts a *zenith-angle-dependent coherence loss* that is *independent of energy* (for fixed χ_k). This contrasts with absorption models, which predict energy-dependent disappearance. Hyper-K's large statistics ($\sim 10^6$ atmospheric events over 10 years) can resolve $\mathcal{O}(10^{-5})$ fractional deviations in zenith-angle bins.

Falsification criterion:

1. If Hyper-K finds *no zenith-angle-dependent suppression* beyond standard MSW, SymC envelope is constrained to $\Gamma_{\text{eff}} < 10^{-24}$ GeV in Earth's interior.
2. If Hyper-K observes zenith-dependent coherence loss scaling with matter path length and exhibiting the predicted χ_k hierarchy (stronger suppression for lower-mass states), this validates SymC.

Timeline: Hyper-K commissioning 2027; atmospheric neutrino analysis ongoing through 2035.

D. MSW resonance structure and exceptional-point traversal (Solar neutrinos, ongoing)

Observable: Solar ν_e survival probability $P_{ee}(E)$ across $E \sim 0.2$–15 MeV.

Standard prediction: MSW resonance in Sun produces adiabatic flavor conversion; smooth $P_{ee}(E)$ curve.

SymC prediction: MSW resonance occurs at *local* $\chi = 1$ (exceptional point). For solar densities transitioning from core ($\rho \sim 150$ g/cm^3) to surface, the EP locus shifts relative to the Hermitian resonance $\Delta m^2 \cos 2\theta = 2EV_e$ due to finite $\Gamma_f(x)$. This shift is $\mathcal{O}(\Gamma_{\text{eff}}/\Delta m^2)$ and produces a *spectral distortion* in $P_{ee}(E)$ near $E \sim 3$ MeV (where Δm^2_{21} resonance occurs).

Falsification criterion: Current solar neutrino data (SNO, Super-K, Borexino) constrain $P_{ee}(E)$ to $\sim 5\%$ precision. If future precision measurements (e.g., JUNO solar analysis) resolve spectral features consistent with EP-shifted resonance, this supports SymC. Absence of such features constrains Γ_{eff} in solar matter.

Timeline: Ongoing; JUNO solar neutrino program aims for $< 3\%$ precision by 2028.

E. Nonunitarity tests via global fits (2025–2030)

Observable: Effective mixing matrix U_{eff} derived from combined reactor, accelerator, and atmospheric data.

Standard prediction: U is unitary; $\|UU^\dagger - I\|_\infty < 10^{-2}$ (current bound).

SymC prediction: Biorthogonal U_{eff} from non-Hermitian Γ_m produces $\|U_{\text{eff}}U^\dagger_{\text{eff}} - I\|_\infty \sim 10^{-4}$ for terrestrial densities (as calculated in Section V). This is *below* current sensitivity but *above* projected DUNE+Hyper-K combined sensitivity ($\sim 10^{-3}$ by 2030).

Falsification criterion: If future global fits find $\|U_{\text{eff}}U^\dagger_{\text{eff}} - I\|_\infty > 10^{-3}$ with pattern matching SymC's χ_k hierarchy, this is evidence for open-system dynamics. If unitarity holds to $< 10^{-4}$, this constrains Γ_{eff} in all measured environments.

Timeline: Global fit updates annual; decisive constraints by 2030 with DUNE+Hyper-K data.

F. Sterile neutrino stability bounds (2025–2028)

Observable: Short-baseline anomalies (LSND, MiniBooNE) vs null results (MicroBooNE).

Standard prediction: Unconstrained sterile mixing; data tension remains unresolved.

SymC prediction: Four-flavor stability requires $\eta_{\text{tot}}^{(4)}$ optimization. Adding a sterile state ν_s with mass $m_s \sim 1$ eV introduces $\chi_s = \Gamma_{\text{eff}}/(2\varpi_s)$. For $m_s^2 \sim 1$ eV^2 and $E = 1$ GeV, $\varpi_s = 5 \times 10^{-19}$ GeV, giving $\chi_s = 2 \times 10^{-5}$ (strongly underdamped). However, if sterile mixing angles are large ($|U_{e4}|^2 \gtrsim 0.01$), the effective $\Gamma_m^{(4)}$ acquires significant off-diagonal terms, destabilizing the system unless $\eta_{\text{tot}}^{(4)}$ remains near maximum. This imposes a *stability-based upper bound* on $|U_{e4}|^2$.

Falsification criterion: If short-baseline experiments confirm large sterile mixing ($|U_{e4}|^2 > 0.03$) that violates SymC stability bounds, the framework is falsified. If sterile mixing is constrained to levels consistent with $\eta_{\text{tot}}^{(4)}$ optimization, SymC predictive power is validated.

Timeline: MicroBooNE final results released; next-generation SBN program (SBND, ICARUS) ongoing through 2028.

Summary of experimental falsification

The SymC neutrino framework is falsifiable on *multiple independent fronts* within 2–6 years:

- **2025–2027:** JUNO reactor spectrum tests matter-segment envelope at $\mathcal{O}(10^{-7})$.
- **2027–2030:** Hyper-K atmospheric neutrinos test zenith-dependent coherence loss at $\mathcal{O}(10^{-5})$.
- **2028–2031:** DUNE ND/FD ratio tests baseline-dependent suppression and χ_k hierarchy at $\mathcal{O}(10^{-6})$.
- **2025–2030:** Global fits constrain nonunitarity; decisive by 2030.
- **2025–2028:** Short-baseline sterile searches test stability bounds.
- **Ongoing:** Solar neutrino precision tests EP-shifted MSW resonance.

Appendix A: Origin of the second-order form (from GKSL)

Starting with the GKSL master equation $\dot{\rho} = -i[H, \rho] + \sum_a \mathcal{D}[L_a]\rho$ and flavor-basis jump operators $L_\alpha = \sqrt{\gamma_\alpha}\, |\alpha\rangle \langle\alpha|$, the single-particle Schrödinger picture acquires an effective

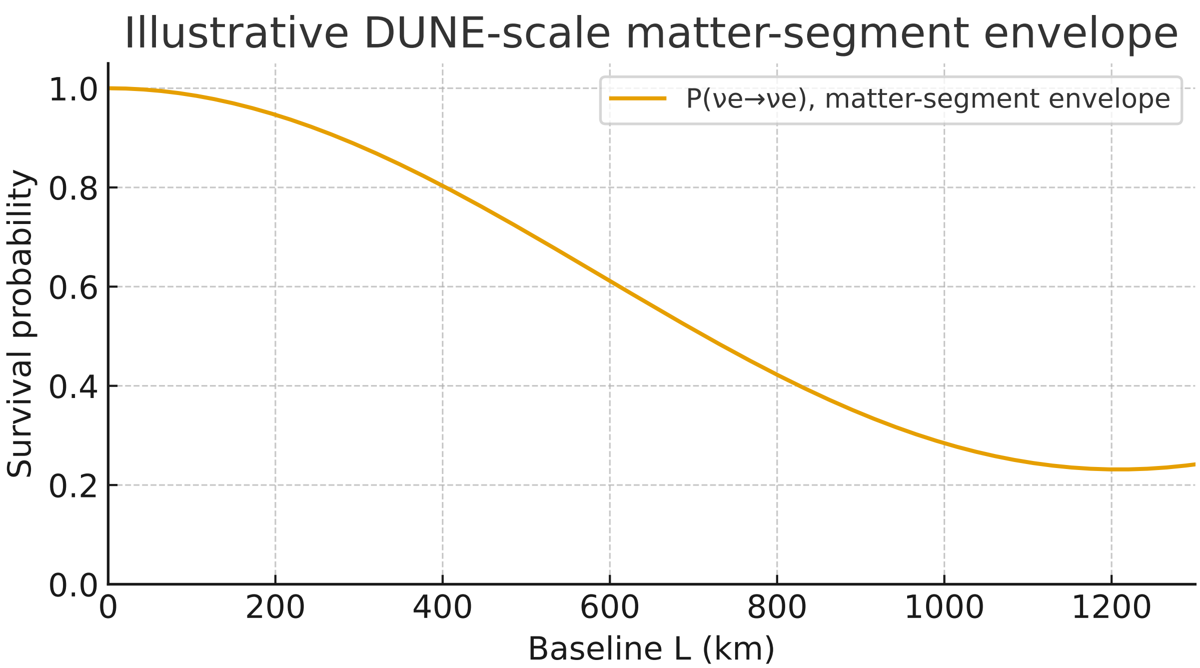

Figure 1: Matter-segment prediction (DUNE-like). Illustrative $P(\nu_\mu \to \nu_e)$ across a constant-density segment with representative Γ_{eff}. Vacuum segments use Eq. (1) exactly (no envelope); damping appears only inside matter.

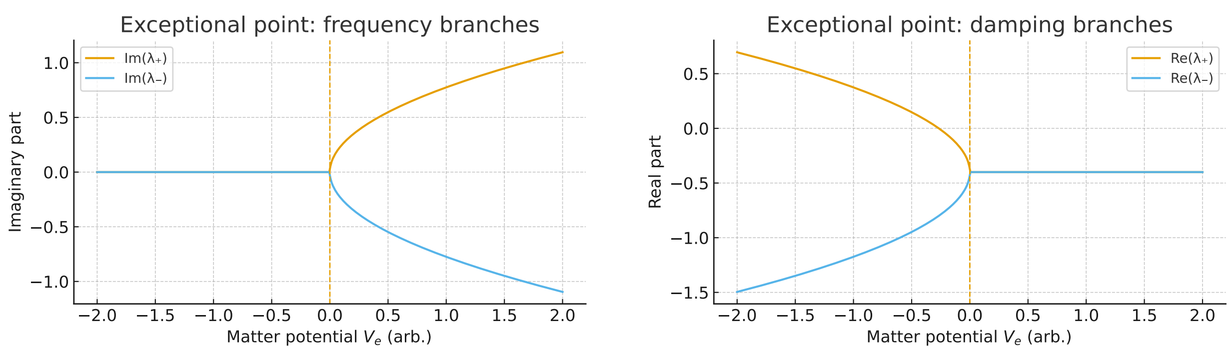

(a) Im parts vs V_e

(b) Re parts vs V_e

Figure 2: Two-state EP demonstration. Clean coalescence in the quadratic eigenproblem near MSW; flavor-dependent damping shifts the discriminant locus.

non-Hermitian term $i\dot{\nu}_f = (H - i\Gamma_f/2)\nu_f$. Eliminating $\dot{\nu}_f$ between the real and imaginary parts produces the closed second-order equation

$$\ddot{\nu}_f + \Gamma_f \dot{\nu}_f + \left(\Omega_f^2 + 2EV_f\right)\nu_f = 0,$$

valid in the weak-coupling/Markov limit used here.

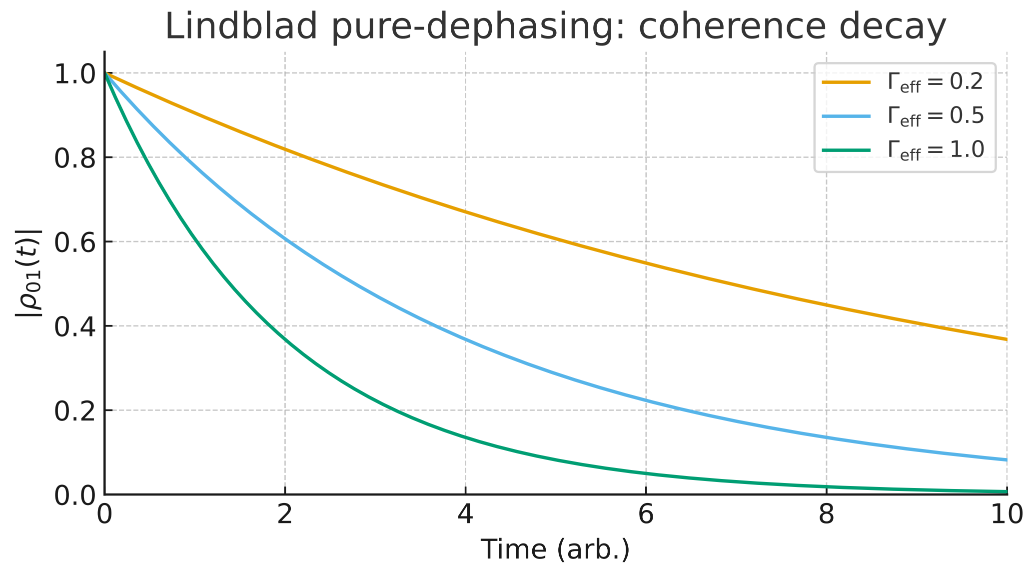

Figure 3: Minimal Lindblad demonstration. Pure dephasing attenuates interference terms while preserving trace; the coherence amplitude monotonically decreases.

Appendix B: Quadratic eigenproblem and EP criterion

The normal-mode ansatz $\nu_m(t) = ve^{\lambda t}$ in $\ddot{\nu}_m + \Gamma_m \dot{\nu}_m + \Omega_m^2 \nu_m = 0$ gives

$$(\lambda^2 I + \lambda\,\Gamma_m + \Omega_m^2)\,v = 0.$$

For a scalar mode with $(\Gamma_m)_{kk} = \Gamma$ and $(\Omega_m^2)_{kk} = \Omega^2$,

$$\lambda_\pm = -\frac{\Gamma}{2} \pm \sqrt{\Omega^2 - \frac{\Gamma^2}{4}} = -\chi|\Omega| \pm i\,|\Omega|\sqrt{1-\chi^2}, \quad \chi \equiv \frac{\Gamma}{2|\Omega|}.$$

Near an MSW resonance the dynamics reduce to a two-dimensional subspace with polynomial $f(\lambda) = \det(\lambda^2 I + \lambda\,\Gamma_2 + \Omega_2^2)$. An exceptional point occurs when $f(\lambda^\star) = 0$ and $\partial_\lambda f(\lambda^\star) = 0$ share a root.

Appendix C: Lindblad mapping and envelope interpretation

Flavor-basis dephasing produces decay of off-diagonal density-matrix elements while preserving trace. In the weak-coupling/Markov limit the interference terms acquire an exponential attenuation consistent with an effective envelope *inside matter segments* determined by $\Gamma_f(x)$;

in pure vacuum segments no envelope is applied.

Reproducibility and data/code availability

All figures were generated with scripts included in the companion code bundle. Parameter files specify PMNS values, energy settings, and $\Gamma_f(x)$ profiles used for each panel. Zenodo archive (code + parameter JSON + figure notebooks): **[insert Zenodo DOI here]**. Script names: `make_survival_matter.py`, `make_EP_scan.py`, `make_lindblad_decay.py`. Figures are embedded as vector PDFs at publication resolution.

References

1. B. Pontecorvo, "Mesonium and anti-mesonium," *Sov. Phys. JETP* **6**, 429 (1957).
2. Z. Maki, M. Nakagawa, and S. Sakata, "Remarks on the unified model of elementary particles," *Prog. Theor. Phys.* **28**, 870 (1962).
3. L. Wolfenstein, "Neutrino oscillations in matter," *Phys. Rev. D* **17**, 2369 (1978).
4. S.P. Mikheyev and A.Yu. Smirnov, "Resonant amplification of neutrino oscillations in matter and solar neutrino spectroscopy," *Sov. J. Nucl. Phys.* **42**, 913 (1985).
5. G. Raffelt, *Neutrinos and the Early Universe*, Oxford University Press (1996).
6. C. Giunti and C.W. Kim, *Fundamentals of Neutrino Physics and Astrophysics*, Oxford University Press (2007).
7. M. Bustamante and S. Pakvasa, "Decoherence and damping in high-energy neutrino oscillations," *Phys. Rev. D* **93**, 093013 (2016).
8. F. Benatti and R. Floreanini, "Open system approach to neutrino oscillations," *JHEP* **02**, 032 (2001).
9. E. Lisi, A. Marrone, and D. Montanino, "Probing possible decoherence effects in atmospheric neutrino oscillations," *Phys. Rev. Lett.* **85**, 1166 (2000).
10. M. Blasone, G. Lambiase, and G. Vitiello, "Quantum field theory of three-flavor neutrino mixing and oscillations with CP violation," *Phys. Rev. D* **97**, 105008 (2018).

11. W. D. Heiss, "The physics of exceptional points," *J. Phys. A: Math. Theor.* **45**, 444016 (2012).

12. A. Mostafazadeh, "Pseudo-Hermiticity versus PT symmetry: The necessary condition for the reality of the spectrum of a non-Hermitian Hamiltonian," *J. Math. Phys.* **43**, 205–214 (2002).

13. P. D. Mannheim, "Antilinearity rather than Hermiticity as a guiding principle for quantum theory," *J. Phys. A: Math. Theor.* **51**, 315302 (2018).

14. Z. Gong, Y. Ashida, K. Kawabata, K. Takasan, S. Higashikawa, and M. Ueda, "Topological phases of non-Hermitian systems," *Phys. Rev. X* **8**, 031079 (2018).

15. H.-P. Breuer and F. Petruccione, *The Theory of Open Quantum Systems*, Oxford University Press (2002).

16. DUNE Collaboration, "Long-baseline neutrino oscillation physics potential of DUNE," *Phys. Rev. D* **108**, 032005 (2023).

17. JUNO Collaboration, "JUNO physics and detector overview," *Prog. Part. Nucl. Phys.* **123**, 103927 (2022).

18. Hyper-Kamiokande Proto-Collaboration, "Hyper-Kamiokande Design Report," *arXiv:1805.04163* (2018).

19. Super-Kamiokande Collaboration, "Solar neutrino measurements in Super-Kamiokande-IV," *Phys. Rev. D* **94**, 052010 (2016).

20. IceCube Collaboration, "Measurement of atmospheric neutrino oscillations at 6–56 GeV with IceCube DeepCore," *Phys. Rev. Lett.* **120**, 071801 (2020).

21. I. Esteban *et al.*, "The fate of hints: updated global analysis of three-flavor neutrino oscillations," *JHEP* **09**, 178 (2024).